

Can Isolated Single Black Holes Produce X-ray Novae?

Tatsuya Matsumoto,^{1*} Yuto Teraki,^{2,3} and Kunihiro Ioka²

¹*Department of Physics, Graduate School of Science, Kyoto University, Kyoto 606-8502, Japan*

²*Center for Gravitational Physics, Yukawa Institute for Theoretical Physics, Kyoto University, Kyoto 606-8502, Japan*

³*National Institute of Technology, Asahikawa College, Asahikawa 071-8142, Japan*

Accepted XXX. Received YYY; in original form ZZZ

ABSTRACT

Almost all black holes (BHs) and BH candidates in our Galaxy have been discovered as soft X-ray transients, so-called X-ray novae. X-ray novae are usually considered to arise from binary systems. Here we propose that X-ray novae are also caused by isolated single BHs. We calculate the distribution of the accretion rate from interstellar matter to isolated BHs, and find that BHs in molecular clouds satisfy the condition of the hydrogen-ionization disk instability, which results in X-ray novae. The estimated event rate is consistent with the observed one. We also check an X-ray novae catalog and find that 16/59 \sim 0.27 of the observed X-ray novae are potentially powered by isolated BHs. The possible candidates include *IGR J17454-2919*, *XTE J1908-094*, and *SAX J1711.6-3808*. Near infrared photometric and spectroscopic follow-ups can exclude companion stars for a BH census in our Galaxy.

Key words: black hole physics – stars: black holes – ISM: clouds – X-rays: stars

1 INTRODUCTION

X-ray novae are soft X-ray transient events with ~ 10 days of rapid brightening up to $\sim 10^{38}$ erg s⁻¹, followed by exponential decays (see Tanaka & Shibazaki 1996; Chen et al. 1997; Yan & Yu 2015, for reviews). X-ray novae are considered to be produced by binary systems composed of low mass stars and compact objects such as neutron stars or black holes (BHs), so-called a low mass X-ray binary (LMXB) system. About twenty LMXBs have been dynamically confirmed to contain BHs through spectral observations of companion stars. Furthermore, 30-40 of X-ray novae share the same X-ray signatures with those of BH LMXB systems, but they are too faint after an outburst to conduct follow-up observations (Corral-Santana et al. 2016). Therefore, strictly speaking, it is unclear whether these X-ray novae without follow-up observations are really produced by binary systems or not.

In the standard scenario, X-ray novae are explained by the hydrogen-ionization instability of accretion disks (a kind of thermal-viscous instability, see Lasota (2001), for a review). The instability model is originally proposed as a mechanism of dwarf novae, which are optical transients caused by white dwarf binary systems (Osaki 1974; Hōshi 1979), and later applied to X-ray novae (van Paradijs & Verbunt 1984; Cannizzo et al. 1985; Huang & Wheeler 1989; Mineshige & Wheeler 1989). When a region in a disk has low temperature for hydrogen to recombine, the negative hydrogen (H⁻) ions dominate the

opacity. As opposed to the free-free opacity, the H⁻ hydrogen opacity is a steep increasing function of temperature. This rapid response to the temperature change makes an S-shaped structure in the thermal equilibrium curve of the region (see Fig 1). In the quiescent phase, the region is in the low temperature branch, while when the surface density reaches a critical value, the region makes a transition to a hot branch and increases the mass accretion rate. Then, the inner annulus is also heated, and the whole disk mass accretes to the central object. This is the origin of X-ray brightening.

Recently, the advanced Laser Interferometer Gravitational Observatory (LIGO) has detected gravitational waves (GWs) and observed binary BH mergers for the first time (Abbott et al. 2016a,c,d). If such merged spinning BHs exist in our Galaxy, they can be high energy sources (Ioka et al. 2017). Before the GW detections, isolated BHs are also believed to reside in our Galaxy. Based on the stellar evolution theory, the number of isolated BHs is as many as $\sim 10^8$ (Shapiro & Teukolsky 1983), some authors have discussed high energy phenomena caused by isolated BHs (Armitage & Natarajan 1999; Barkov et al. 2012; Teraki et al. 2017), and studied the detectability of isolated BHs (Fujita et al. 1998; Agol & Kamionkowski 2002; Fender et al. 2013; Matsumoto et al. 2017). However, because of the very low mass accretion rate, the accretion disks around BHs are radiatively inefficient (Narayan & Yi 1994) and the detection of isolated BHs is challenging if BHs are stationary sources.

In this paper, we propose a novel idea that isolated sin-

* E-mail: matsumoto@tap.scphys.kyoto-u.ac.jp

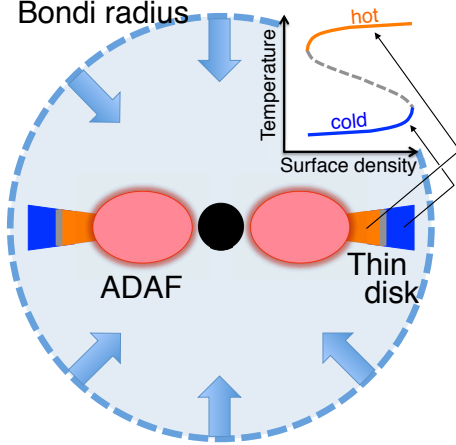


Figure 1. Schematic picture of an isolated BH with a thin disk part attached to inner ADAF part. The thin disk part consists of an outer cold branch and an inner hot branch in the S-shaped thermal equilibrium curve (upper right).

gle BHs in our Galaxy can produce transient events like X-ray novae. The structure of this paper is as follows. First, we calculate the mass accretion distribution of isolated BHs (section 2). Next, we find that some BHs in molecular clouds accrete enough mass to have a thin disk part in section 3. This is because for a large mass accretion rate, a disk has a high density enough to cool by radiation and become geometrically thin at the outer part of the disk (Abramowicz et al. 1995; Narayan & Yi 1995). In Fig 1, we show a schematic picture of the system we consider. The thin disk region can suffer from the hydrogen-ionization instability and cause transient events like X-ray novae. We also estimate that the event rate is comparable to that of the observed X-ray novae. Finally, we suggest that some X-ray novae without companions could be produced by isolated BHs in section 4. We also discuss how to discriminate an isolated BH from a binary by observations.

2 ACCRETION RATE DISTRIBUTION OF ISOLATED BHS

In this section, we consider the mass accretion onto Galactic isolated BHs. The BHs accrete interstellar medium (ISM) gas and form accretion disks. We study the accretion rate distribution of isolated BHs taking the BH mass, the BH velocity, and the ISM density distributions into account.

An isolated BH pulls the ISM gas by its gravity and accretes the gas via so-called Bondi accretion (Hoyle & Lyttleton 1939; Bondi & Hoyle 1944; Bondi 1952). The Bondi radius and the accretion rate are estimated as

$$R_B = \frac{GM}{c_s^2 + v^2} \quad (1)$$

$$\approx 8.3 \times 10^{13} \left(\frac{M}{10 M_\odot} \right) \left(\frac{V}{40 \text{ km s}^{-1}} \right)^{-2} \text{ cm}, \quad (2)$$

$$\dot{M}_B = 4\pi R_B^2 \rho V \quad (3)$$

$$\approx 8.2 \times 10^{11} \left(\frac{M}{10 M_\odot} \right)^2 \left(\frac{V}{40 \text{ km s}^{-1}} \right)^{-3} \left(\frac{n}{1 \text{ cm}^{-3}} \right) \text{ g s}^{-1} \quad (4)$$

where, G , M , v , c_s , and ρ are the gravitational constant, the

BH mass, the BH velocity, the sound speed of ISM, and the mass density of ISM, respectively. We define the velocity V as $V := \sqrt{c_s^2 + v^2}$. From Eq. (3) to Eq. (4), we convert the mass density to the number density n by using the relation $\rho = m_u \mu n$, where m_u and $\mu = 1.41$ are the atomic mass unit and the mean molecular weight. It should be noted that the Bondi accretion rate is much smaller than the Eddington accretion rate defined as

$$\dot{M}_{\text{Edd}} = \frac{4\pi GMm_p}{\eta\sigma_T c} \quad (5)$$

$$\approx 1.4 \times 10^{19} \left(\frac{M}{10 M_\odot} \right) \text{ g s}^{-1}, \quad (6)$$

where m_p , $\eta = 0.1$, σ_T and c are the proton mass, radiative efficiency¹, Thomson cross section, and the speed of light, respectively.

The accreting matter forms an accretion disk at the centrifugal radius (Shapiro & Lightman 1976). In the Bondi accretion, the accreting gas is assumed to have a spherical or axial symmetry. However, the actual ISM has density and turbulent velocity fluctuations. Because of the difference of the density and the turbulent velocity in the scale of the Bondi radius, the accreting ISM has a specific angular momentum of

$$l = \frac{1}{4} \left[\frac{\delta\rho}{\rho} + 2 \frac{\delta V}{V} \right] R_B V. \quad (7)$$

The quantities $\delta\rho/\rho$ and $\delta V/V$ are evaluated at the Bondi radius length scale ($\sim 2R_B$). For the former quantity, we use the observed density fluctuation as $\delta\rho/\rho \approx (R/6 \times 10^{18} \text{ cm})^{1/3}$ (Armstrong et al. 1995; Draine 2011). This scaling holds at smaller length scale than the Bondi radius. The latter quantity is evaluated by using the correlation of the turbulent velocity dispersion and the length scale in the molecular clouds, so-called Larson's first law as (Larson 1981; Heyer & Brunt 2004), $\delta v_{\text{turb}} \approx 1(R/1 \text{ pc})^{1/2} \text{ km s}^{-1}$. For slowly moving isolated BHs with velocity of $V \sim c_s \sim 10 \text{ km s}^{-1}$, the contribution from the velocity fluctuation is evaluated as $\delta V/V \sim \delta v_{\text{turb}}/c_s \sim 0.1(R/1 \text{ pc})^{1/2}$. At the Bondi radius, we see that the velocity fluctuation is much smaller than the density fluctuation. Therefore, the disk radius is largely determined by the density fluctuation.

Then, at the centrifugal radius, the gas starts to circulate and forms an accretion disk. The disk size is evaluated by the centrifugal radius as

$$R_d := \frac{l^2}{GM} \quad (8)$$

$$\approx 4.7 \times 10^9 \left(\frac{M}{10 M_\odot} \right)^{5/3} \left(\frac{V}{40 \text{ km s}^{-1}} \right)^{-10/3} \text{ cm}. \quad (9)$$

Since the mass accretion rate is much smaller than the Eddington rate, the accretion disk cools with not radiation but advection, so-called advection dominated accretion flow (ADAF, Narayan & Yi 1994).

When magnetic fields from the ISM thread the accretion disk, the magnetic braking effect may work and reduce the disk radius. Since the efficiency of the braking effect

¹ Some literatures define the Eddington accretion rate without the radiative efficiency η . It should also be noted that the name “radiative efficiency” does not mean the true efficiency.

sensitively depends on the geometry of the magnetic fields (Mouschovias 1985, and references therein), it is difficult to study whether the magnetic braking affects the disk radius. Here, we estimate the timescale of the angular momentum transfer by the Alfvén crossing timescale at a given radius R , and compare it with the free fall timescale $t_{\text{ff}} = \sqrt{R^3/GM}$. At the Bondi radius $R_{\text{B}} \approx 1.3 \times 10^{15}$ cm for an isolated BHs with the velocity $V \approx 10 \text{ km s}^{-1}$, each timescale is evaluated as $t_{\text{A}} \approx 1.0 \times 10^{10}$ s and $t_{\text{ff}} \approx 1.3 \times 10^9$ s for the magnetic field and the density at the Bondi radius of $B \approx 10 \mu\text{G}$ (Crutcher et al. 2010) and $n \approx 10^2 \text{ cm}^{-3}$. These are the typical values in molecular clouds, where isolated BHs get enough accretion rate to power X-ray novae (see below). Then, we can neglect the braking effect. At the disk radius $R_{\text{d}} \approx 4.8 \times 10^{11}$ cm, each timescale is estimated as $t_{\text{A}} \approx 5.7 \times 10^5$ s and $t_{\text{ff}} \approx 9.2 \times 10^3$ s, where we use the flux freezing $BR^2 = \text{const}$ and the disk density given by Eq. (33). Therefore, it is unlikely that the braking effect transfers a significant amount of angular momentum, and reduces the disk radius. In order to study this effect in detail, we may need to conduct a magnetohydrodynamic simulation, but it is beyond of the scope of this work.

For a stationary accretion disk to exist, the infall time at the Bondi radius $t_{\text{ff}}(R_{\text{B}})$ should be shorter than the dynamical time of a BH to cross the Bondi radius $t_{\text{dyn}} := 2R_{\text{B}}/v$. This condition is achieved as $t_{\text{ff}}(R_{\text{B}})/t_{\text{dyn}} = v/2V \approx 0.35 \lesssim 1$, where we set the BH velocity is equal to the sound velocity $v \approx c_s$.

We calculate the mass accretion distribution function of Galactic isolated BHs. The accreting ISM gas has several phases with different densities. BHs also have velocity and mass distributions. Therefore, we have to take into account for these statistical properties. By using the normalized mass and accretion rate defined as $m := M/M_{\odot}$ and $\dot{m} := \dot{M}/\dot{M}_{\text{Edd}}$, the mass accretion distribution is given by (Agol & Kamionkowski 2002; Ioka et al. 2017)

$$\frac{dN}{dm} = N \int dm \frac{dp(m)}{dm} \int dv \frac{df(v)}{dv} \int dn \frac{d\xi(n)}{dn} h(m, v) \delta(\dot{m}(n, m, v) - \dot{m}), \quad (10)$$

where N , $dp(m)/dm$, $df(v)/dv$, $d\xi(n)/dn$, and $h(m, v)$ are the total isolated BH number, the BH mass, the BH velocity and the ISM density distribution functions, and a correction factor due to the scale height of the ISM phase and the BH distribution. We set the total number as $N = 10^8$ (Shapiro & Teukolsky 1983). We can integrate Eq. (10) over v and obtain

$$\frac{dN}{dm} = N \int dm \frac{dp(m)}{dm} \int dn \frac{df(v_0)}{dv} \frac{d\xi(n)}{dn} h(m, v_0) \frac{V^2|_{v=v_0}}{3v_0\dot{m}}, \quad (11)$$

where v_0 is given by

$$v_0^2 = \left(\frac{GMc\eta\sigma_{\text{T}}\mu}{\dot{m}} \right)^{2/3} - c_s^2. \quad (12)$$

We briefly explain the BH mass, the BH velocity, and the ISM density distribution functions. These functions are the same as those used in Ioka et al. (2017). For the BH mass distribution function, we assume a Salpeter-like mass function as,

$$\frac{dp(m)}{dm} = Cm^{-\gamma}, \quad (m_{\text{min}} < m < m_{\text{max}}), \quad (13)$$

where $\gamma = 2.35$ and we normalize the mass function as $\int dm \frac{dp(m)}{dm} = 1$ by setting $C = (\gamma - 1)/(m_{\text{min}}^{1-\gamma} - m_{\text{max}}^{1-\gamma})$. We set the upper and lower mass as $m_{\text{min}} = 5 M_{\odot}$ and $m_{\text{max}} = 15 M_{\odot}$. The maximum BH mass is motivated by the stellar evolution calculation for the solar abundance (Belczynski et al. 2010). It should be noted that more massive BHs of $\sim 50 M_{\odot}$ could form in low metallicity environments, as suggested by the GW observations (Abbott et al. 2016b). The number of the massive population could be comparable to that for the solar abundance because the duration of the low metal era is about tenth of the cosmic time, but the star formation rate is also ten times larger than now (Snaith et al. 2014; Haywood et al. 2016). Although considering their contribution is interesting, we do not take them into account because our result does not depend on the maximum BH mass so much.

In this work, we assume a Maxwellian velocity distribution as,

$$\frac{df(v)}{dv} = \sqrt{\frac{2}{\pi}} \frac{v^2}{\sigma_v^3} \exp\left(-\frac{v^2}{2\sigma_v^2}\right), \quad (14)$$

where σ_v is the velocity dispersion. We set this value as $\sigma_v = 40 \text{ km/s}$. This is motivated by the observed scale height of low mass X-ray binaries from the Galactic plane (White & van Paradijs 1996). Recently, Repetto et al. (2012) have suggested that BHs also receives natal kicks at births and the kick velocity can be the same as those received by neutron stars ($\sim 200 - 400 \text{ km s}^{-1}$). They also used the distance of the binaries from the Galactic plane to deduce the conclusion. However, it should be noted that these arguments depend sensitively on the errors in the evaluated distances. In order to get reliable distance or velocity values, we need more precise measurements such as astrometric observations (Miller-Jones 2014). Such astrometric observations have been applied only for one BH X-ray binary system, Cyg X-1, which has a low proper velocity as $\sim 20 \text{ km s}^{-1}$ (Chevalier & Ilovaisky 1998; Mirabel & Rodrigues 2003; Reid et al. 2011).

We consider five types of the ISM phase: molecular clouds, cold H_{I} , warm H_{I} , warm H_{II} , and hot H_{II} mediums. For molecular clouds and cold H_{I} medium, we adopt the power law distribution as (Berkhuijsen 1999),

$$\frac{d\xi(n)}{dn} = D\xi_0 n^{-\beta}, \quad (n_1 < n < n_2). \quad (15)$$

We normalize the function as $\int dn \frac{d\xi(n)}{dn} = \xi_0$ by choosing the constant $D = (\beta - 1)/(n_1^{1-\beta} - n_2^{1-\beta})$, where ξ_0 is the volume filling factor of the phase in the Galactic volume. The power law index β and the upper and lower density n_1 and n_2 are shown in Table 1. For the warm H_{I} , warm H_{II} , and hot H_{II} mediums, we do not consider the density distribution but assume a uniform density with their typical values. Then, we use the delta function for these phases as

$$\frac{d\xi(n)}{dn} = \xi_0 \delta(n - n_1). \quad (16)$$

We take the value of the mean molecular weight as $\mu = 2.82$ for the molecular clouds and $\mu = 1.41$ for the other phases with the Milky Way abundance (Kauffmann et al. 2008).

We comment the uncertainty of the density distribution function of molecular clouds because molecular clouds are the main site where isolated BHs launch X-ray novae.

Table 1. The parameters for each ISM phase. For molecular clouds and cold H_I medium which have broad density distributions, the minimum n_1 , maximum n_2 number densities, and power law index of the distributions β are shown. For the other mediums, we show the typical density in the column 2. We represent the volume filling factors ξ_0 , the sound velocities c_s , and scale heights H_d in column 5, 6, 7, respectively. For the sound velocity, we include the contribution of the turbulent velocity.

| phase | n_1 [cm ⁻³] | n_2 [cm ⁻³] | β | ξ_0 | c_s [km s ⁻¹] | H_d [kpc] |
|----------------------|---------------------------|---------------------------|---------|------------------|-----------------------------|-------------|
| Molecular cloud | 10 ² | 10 ⁵ | 2.8 | 10 ⁻³ | 10 | 0.075 |
| Cold H _I | 10 | 10 ² | 3.8 | 0.04 | 10 | 0.15 |
| Warm H _I | 0.3 | - | - | 0.35 | 10 | 0.5 |
| Warm H _{II} | 0.15 | - | - | 0.2 | 10 | 1 |
| Hot H _{II} | 0.002 | - | - | 0.4 | 150 | 3 |

The power law distribution is obtained by the mass function of molecular clouds $dN_{cl}/dM_{cl} \propto M_{cl}^{-p}$, where N_{cl} and M_{cl} are the number of molecular clouds and the molecular cloud mass, and the density and cloud size relation (so-called Larson’s third law, [Larson 1981](#)), $nR_{cl} \propto R_{cl}^q$, where R_{cl} is the molecular cloud size. While the observed typical indices of $p = 1.6$ ([Williams & McKee 1997](#)) and $q = 0$ ([Solomon et al. 1987](#)) give $\beta = 2.8$, the inaccuracy of these index value may also cause an uncertainty of our result. By the observations, the indices are determined within the range of $p \simeq 1.5 - 1.8$ ([Kramer et al. 1998](#); [Rosolowsky 2005](#)) and $q \simeq 0 - 0.1$ ([Heyer et al. 2009](#)), which result in the index $\beta \simeq 3.0 - 2.4$. However, this change of β increases or decreases only the maximum accretion rate ($\dot{m} \simeq 2 \times 10^{-2}$, see Fig 2) and does not change seriously the total number of BHs which power X-ray novae. Therefore, our main results such as the event rate does not sensitively depend on the uncertainty of the density distribution functions. In addition to the density distribution, the turbulent velocity distribution may change the accretion distribution. Note that we include this contribution into the sound velocity (see the caption in Table 1). The Larson’s first law shows that the smaller cloud has the smaller turbulent velocity, which makes the BH accretion rate large. However, according to the Larson’s third law, these clouds have also large density and only change the maximum accretion rate.

Finally, we explain the correction factor $h(m, v)$. For a given BH velocity, we can evaluate the BH’s scale height by assuming the Galactic potential. We use the following simple potential model as,

$$v_z^2 = v^2/3 \quad (17)$$

$$\frac{1}{2}v_z^2 = \Phi[H(v_z)] \quad (18)$$

$$\frac{\Phi(z)}{2\pi G} = K \left(\sqrt{z^2 + Z^2} - Z \right) + Fz^2, \quad (19)$$

where $Z = 180 \text{ pc}$, $K = 48 M_\odot \text{ pc}^{-2}$, and $F = 0.01 M_\odot \text{ pc}^{-3}$ ([Kuijken & Gilmore 1989a,b](#)). When the derived scale height $H(v_z)$ is larger than the scale height of the ISM phase H_d , we correct the count by multiplying $H_d/H(v_z)$. Then, the correction factor is given by

$$h(m, v) = \min \left[1, \frac{H_d}{H(v_z)} \right]. \quad (20)$$

We compile the distribution functions discussed above, and integrate Eq. (11) numerically. In Fig 2, we show the mass accretion distribution of Galactic isolated BHs. The vertical and horizontal axes show the number of BHs and

the normalized mass accretion rate, respectively. The normalized accretion rate relates with the BH mass, the BH velocity, and the ISM density as

$$\dot{m} \simeq 5.8 \times 10^{-8} \left(\frac{M}{10 M_\odot} \right) \left(\frac{V}{40 \text{ km s}^{-1}} \right)^{-3} \left(\frac{n}{1 \text{ cm}^{-3}} \right), \quad (21)$$

where we use Eqs. (3) and (5). The orange-red, dark-blue, magenta, light-green, and turquoise curves show the number distributions of isolated BHs in the molecular clouds, cold H_I, warm H_I, warm H_{II}, and hot H_{II} mediums, respectively.

Let us discuss the shape of the distribution functions in Fig 2. The peak value of the distribution in each ISM medium is roughly evaluated by $N_{\text{peak}} \sim N \xi_0 h$. For the hot H_{II} medium, the distribution shows a peaky shape. This is because the hot H_{II} medium has a larger sound velocity c_s than the typical BH velocity $v \sim \sigma_v$, and the distribution reflects only the BH mass distribution. According to the Galactic potential (19), the BH scale height with the velocity $v \sim \sigma_v = 40 \text{ km s}^{-1}$ is estimated as $H(v_z) \simeq 0.3 \text{ kpc}$. On the other hand, the scale height of the hot H_{II} medium is larger than the BH scale height (see Table 1), and the correction factor reduces to unity $h = 1$. Then, the peak value of the distribution of the hot H_{II} medium is given as $N_{\text{peak}} \sim 4 \times 10^7 (N/10^8)(\xi_0/0.4)(h/1)$.

For the warm H_I and H_{II} mediums, the mass accretion distributions have a broader shape than that of the hot H_{II} medium because the sound velocities of these mediums are as large as that of the BH velocity, $c_s \lesssim v \sim \sigma_v$. Therefore, the broadness reflects the velocity distribution. These mediums also have larger scale heights than the BH scale height, and have no correction ($h \sim 1$). However, due to the large dispersion, the peak values of the distributions are a bit smaller than the values estimated by $\sim N \xi_0$.

The accretion distributions of the molecular clouds and the cold H_I medium show tails extending to the large accretion rate ($\dot{m} \gtrsim 10^{-5}$ and 10^{-3} , for the cold H_I medium and the molecular clouds, respectively). These tails are attributed to the density distribution. To estimate the peak values of the distributions, we should take the correction factor h into account, because the molecular clouds and the cold H_I medium have smaller scale heights than that of BHs, $H_d < H(v_z)$, which requires corrections of $h \sim 0.1 - 0.3$.

3 X-RAY NOVAE PRODUCED BY ISOLATED BHs

We discuss the possibility that isolated BHs produce X-ray transient events, such as X-ray novae. In section 2,

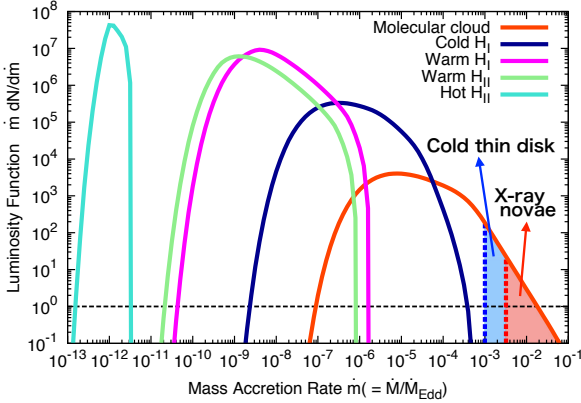


Figure 2. The distribution of the normalized mass accretion rate \dot{m} . Each curve shows the accretion distribution in each medium. The orange-red, dark-blue, magenta, light-green, and turquoise solid curves show the number distribution of isolated BHs in the molecular clouds, cold H I , warm H I , warm H II , and hot H II mediums, respectively. The red and blue dashed lines represent the critical accretion rates required to produce X-ray novae (Eq. 44, for $m = 15$) and to have a standard disk part (Eq. 29, for $m = 15$ and $n = 10^2 \text{ cm}^{-3}$), respectively.

we consider that the accretion disks formed around isolated BHs are ADAFs. However, when the accretion rate is larger than a critical value, the radiative cooling overcomes the advective one and the ADAF becomes a standard disk (Abramowicz et al. 1995). Furthermore, if the standard disk has a low temperature region enough to allow hydrogen to recombine, the disk suffers from the hydrogen-ionization instability and produces an X-ray transient event.

Before discussing the accretion disk structure in detail, we check whether our idea passes the observational constraints. As shown in Fig. 2 and we discuss below, X-ray novae from isolated BHs occur only in molecular clouds because a large accretion rate is necessary. Then, if an X-ray nova is actually powered by an isolated BH, we should detect it in the same direction of a molecular cloud.² We check an X-ray nova catalog (Corral-Santana et al. 2016) and find 17 events in the Galactic plane ($b \lesssim 1.5^\circ$) among 59 X-ray novae ever detected. Comparing the CO emission map in the Galactic plane,³ we find CO emission signatures in the same directions of 16 X-ray novae. Furthermore, the 16 X-ray novae show large column densities of $\sim 10^{22} \text{ cm}^{-2}$ in the soft X-ray spectra, which also support that the 16 X-ray novae are actually accompanied with molecular clouds (see also section 4). We list the 16 candidate X-ray novae in Table 2. The column density and direction are taken from the catalog of Corral-Santana et al. (2016) and references therein. Therefore, we conclude $16/59 \sim 0.27$ of the observed X-ray novae are potentially produced by isolated BHs in molecular clouds.

² Since it is difficult to measure the distance to an X-ray nova only by X-ray observations, we cannot study whether the X-ray nova actually reside in a molecular cloud. Therefore, we only discuss the coincidence of the directions of X-ray novae and molecular clouds.

³ <https://www.cfa.harvard.edu/rtdc/CO/IndividualSurveys/>

When the mass accretion rate is large, an ADAF can accompany a standard disk at the outer part of the disk. This is because at a large radius from the central BH, the radiative cooling rate gets comparable to the advective cooling and viscosity heating rates. We can see this easily by considering the energy equation of ADAFs as

$$(1 - f)q_{\text{vis}} \approx q_{\text{bre}} \quad (22)$$

where q_{vis} and q_{bre} are the viscous heating and the bremsstrahlung cooling rates per volume, respectively. We also assume that the advective cooling rate is approximately given by the viscous heating rate as $q_{\text{adv}} \approx f q_{\text{vis}}$, where f is the efficiency parameter and we set $f = 0.5$ for a fiducial value at the transition region to a standard disk (Narayan & Yi 1995). Then, the left hand side of Eq. (22) represents a net heating rate. By using a self-similar solution of ADAF, we can show that the heating rate depends on radius r as $q_{\text{vis}} \propto r^{-4}$ (Narayan & Yi 1994, 1995), where we normalize a radius by the Schwarzschild radius $R_S = 2GM/c^2$ as $r := R/R_S$. It should be also noted again that we normalize the mass and accretion rate by the solar mass and the Eddington rate as $m := M/M_\odot$ and $\dot{m} := \dot{M}/\dot{M}_{\text{Edd}}$. The bremsstrahlung cooling rate is given by Svensson (1982), and we can show the radius dependence of the cooling rate as $q_{\text{bre}} \propto r^{-7/2}$, where we use the ADAF self-similar solution and assume that electrons have a non-relativistic virial temperature of ions⁴ as (Narayan & Yi 1995; Matsumoto et al. 2017)

$$T_e \approx 3.2 \times 10^{12} \beta_{\text{ADAF}} c_3 r^{-1} \text{ K}. \quad (23)$$

The constants β_{ADAF} and c_3 are the parameters of the ADAF self-similar solution (see below Eq. (25) for more detailed explanation). Then, at a large radius, the radiative cooling rate becomes comparable to the viscous heating rate, and the ADAF becomes a standard disk. Equation (22) is rewritten to the condition for the critical accretion rate at a given radius by using the self-similar solution as (Abramowicz et al. 1995; Narayan & Yi 1995),

$$\dot{m}_{\text{crit}} \approx 2.3 \left(\frac{m_u}{m_e} \right)^{1/2} \frac{\eta}{\alpha_f} \epsilon' (1 - f) c_1^2 c_3 \alpha^2 \beta_{\text{ADAF}}^{-1/2} r^{-1/2} \quad (24)$$

$$\approx 1.4 \times 10^3 \epsilon' (1 - f) c_1^2 c_3 \alpha^2 \beta_{\text{ADAF}}^{-1/2} r^{-1/2} \quad (25)$$

$$\approx 4.4 \times 10^{-1} \left(\frac{\epsilon'}{0.63} \right) \left(\frac{1 - f}{0.5} \right) \left(\frac{c_1}{0.48} \right)^2 \left(\frac{c_3}{0.32} \right) \left(\frac{\alpha}{0.1} \right)^2 \left(\frac{\beta_{\text{ADAF}}}{0.5} \right)^{-1/2} r^{-1/2}, \quad (26)$$

where m_e , α_f , α and β_{ADAF} are the electron mass, the fine structure constant, the viscosity parameter (Shakura & Sunyaev 1973) and the ratio of the gas pressure to the total pressure, respectively. For fiducial values, we set $\alpha = 0.1$ and $\beta_{\text{ADAF}} = 0.5$. The dimensionless constants ϵ' , c_1 , and c_3 appear in the derivation of the ADAF self-similar solution as functions of f , α , and β_{ADAF} (Narayan & Yi 1994, 1995). The notation of these constants is the same as given in Narayan & Yi (1994, 1995), except for β_{ADAF} (where β_{ADAF} is written as β).

⁴ At the outer part of the ADAF ($r \gtrsim 100$), the Coulomb collision works well and makes the electron temperature equal to the ion temperature.

Table 2. Candidates X-ray novae powered by isolated BHs in molecular clouds. ID number corresponds to that used in (Corral-Santana et al. 2016). The column density and direction are taken from (Corral-Santana et al. 2016) and references therein. The column density is evaluated by the absorption signature in the soft X-ray spectra, except for ID47, 28, 22, 11, and, 2, for which the optical extinction formula $N_{\text{H}} = 5.8 \times 10^{21} E(B - V) \text{ cm}^{-2}$ is used (Draine 2011). In the same direction of each event, we find that there is a molecular cloud by checking the CO emission map. NIR counterparts are detected only for ID59, 35, and 34.

| ID | name | $N_{\text{H}} [\text{cm}^{-2}]$ | direction (l, b) | NIR source |
|----|------------------------|----------------------------------|----------------------|------------|
| 59 | IGR J17454-2919 | $1.0\text{--}1.2 \times 10^{23}$ | 359.6444, -00.1765 | ✓ |
| 56 | SWIFT J1753.7-2544 | 5.8×10^{22} | 003.6476, $+00.1036$ | |
| 51 | MAXI J1543-564 | 1.4×10^{22} | 325.0855, -01.1214 | |
| 47 | XTE J1652-453 | 5.1×10^{22} | 340.5297, -00.7867 | |
| 44 | SWIFT J174540.2-290005 | 7.6×10^{22} | 359.9495, -00.0431 | |
| 43 | IGR J17497-2821 | 4.8×10^{22} | 000.9531, -00.4527 | |
| 35 | XTE J1908+094 | 2.3×10^{22} | 043.2615, $+00.4377$ | ✓ |
| 34 | SAX J1711.6-3808 | 2.8×10^{22} | 348.4200, $+00.7880$ | ✓ |
| 28 | XTE J1748-288 | 5.8×10^{22} | 000.6756, -00.2220 | |
| 25 | GRS 1737-31 | 6.0×10^{22} | 357.5880, -00.0990 | |
| 24 | GRS 1739-278 | 1.6×10^{22} | 000.6721, $+01.1758$ | |
| 23 | XTE J1856+053 | 4.5×10^{22} | 038.2690, $+01.2720$ | |
| 22 | GRS 1730-312 | 3.2×10^{22} | 356.6877, $+01.0065$ | |
| 11 | EXO 1846-031 | 3.7×10^{22} | 029.9585, -00.9177 | |
| 8 | H 1743-322 | 2.2×10^{22} | 357.2552, -01.8330 | |
| 2 | 4U 1630-472 | 2.4×10^{22} | 336.9112, $+00.2503$ | |

If $\dot{m} \gtrsim \dot{m}_{\text{crit}}$, the radiative cooling overcomes the advective cooling and no longer the ADAF part exists. Observations of BH X-ray binaries also suggest an outer standard accretion disk truncated in the inner part by radiatively inefficient accretion flow, which can explain some properties of BH X-ray binaries such as the spectral transition between the high-soft state and the low-hard state (Esin et al. 1997; Lasota 2001; Done et al. 2007).

We estimate how many isolated BHs have the standard disk part. We define the transition radius $r_{\text{tr}} (= R_{\text{tr}}/R_{\text{S}})$ by $\dot{m} = \dot{m}_{\text{crit}}(r = r_{\text{tr}})$, where the ADAF part begins to cool radiatively and makes a transition to the standard disk outer-part. By using Eqs. (21) and (25), we obtain the transition radius as,

$$r_{\text{tr}} \approx 1.5 \times 10^9 \left(\frac{m}{10} \right)^{-2} \left(\frac{V}{40 \text{ km s}^{-1}} \right)^6 \left(\frac{n}{10^2 \text{ cm}^{-3}} \right)^{-2}. \quad (27)$$

It should be noted that when we discuss the BHs in molecular clouds, we should use the mean molecular weight of $\mu = 2.82$ in Eq. (21). We use the fiducial values for the ADAF parameters in Eq. (25). In the following, we also use the fiducial values and do not show the dependences of ADAF parameters explicitly. For a disk to have a standard disk part, the transition radius should be smaller than the disk radius $r_{\text{d}} := R_{\text{d}}/R_{\text{S}}$. With Eq. (8), this condition is rewritten to a condition for the velocity V as,

$$V \lesssim 9.2 \left(\frac{m}{10} \right)^{2/7} \left(\frac{n}{10^2 \text{ cm}^{-3}} \right)^{3/14} \text{ km s}^{-1}. \quad (28)$$

Since the velocity is $V > c_{\text{s}} = 10 \text{ km s}^{-1}$, to satisfy the above condition, the BH mass and the density should be larger than the minimum values, $m > 5$ and $n > 10^2 \text{ cm}^{-3}$. Hereafter, we use $m = 15$ for the fiducial value. By substituting Eq. (28) into Eq. (21), we obtain a required minimum accretion rate for an isolated BH to have a standard disk part

as

$$\begin{aligned} \dot{m} \gtrsim \dot{m}_{\text{disk}} = & 1.0 \times 10^{-3} \left(\frac{m}{15} \right)^{1/7} \left(\frac{n}{10^2 \text{ cm}^{-3}} \right)^{5/14} \\ & \left(\frac{\epsilon'}{0.63} \right)^{9/14} \left(\frac{1-f}{0.5} \right)^{9/14} \left(\frac{c_1}{0.48} \right)^{9/7} \\ & \left(\frac{c_3}{0.32} \right)^{9/14} \left(\frac{\alpha}{0.1} \right)^{9/7} \left(\frac{\beta_{\text{ADAF}}}{0.5} \right)^{-9/28}, \quad (29) \end{aligned}$$

where we restore the ADAF parameter dependences. In Fig 2, we show the minimum accretion rate with a blue dashed line for $m = 15$ and $n = 10^2 \text{ cm}^{-3}$.

Next, we discuss the possibility that hydrogen recombines in the thin disk part. We firstly compare the recombination temperature with the temperature in the disk for simplicity, and later discuss the details. The Saha equation gives the hydrogen recombination temperature in the thin disk. When hydrogen is partially ionized, their ionization state determines the abundance of H^- ion (i.e., opacity) (The metal abundance may not change results so much as long as hydrogen mainly supplies electrons). The Saha equation gives the ratio of the ionized hydrogen number density n_{H^+} to the neutral hydrogen density n_{H} as

$$\frac{n_{\text{H}^+} n_{\text{e}}}{n_{\text{H}}} = \frac{(2\pi m_{\text{e}} k_{\text{B}} T)^{3/2}}{h^3} \exp\left(-\frac{\chi_{\text{H}}}{k_{\text{B}} T}\right), \quad (30)$$

where n_{e} , k_{B} , h , and $\chi_{\text{H}} = 13.6 \text{ eV}$ are the electron number density, the Boltzmann constant, the Planck constant, and the hydrogen ionization energy. With the definition of the degree of ionization $x := n_{\text{e}}/(n_{\text{H}} + n_{\text{H}^+})$, and the charge neutrality $n_{\text{e}} = n_{\text{H}^+}$, Eq. (30) is rewritten as

$$\frac{x^2}{1-x} = \frac{(2\pi m_{\text{e}} k_{\text{B}} T)^{3/2}}{n_{\text{H,tot}} h^3} \exp\left(-\frac{\chi_{\text{H}}}{k_{\text{B}} T}\right), \quad (31)$$

where $n_{\text{H,tot}} = n_{\text{H}} + n_{\text{H}^+}$ is the total number density of hydrogen. We simply define the partially ionized state of the hydrogen as $x = 0.5$, which results in the value of the right

hand side of Eq. (31) of 0.5. The temperature and the mass density are given by formulae of the standard disk with gas pressure and free-free absorption (Shakura & Sunyaev 1973; Kato et al. 2008) as

$$T = 1.4 \times 10^8 \alpha^{-1/5} \dot{m}^{-1/5} \dot{m}^{3/10} r^{-3/4} \text{ K} \quad (32)$$

$$\rho = 1.7 \times 10^2 \alpha^{-7/10} \dot{m}^{-7/10} \dot{m}^{11/20} r^{-15/8} \text{ g cm}^{-3}. \quad (33)$$

The total number density of hydrogen is obtained by $n_{\text{H,tot}} = \rho X / m_{\text{p}}$, where $X = 0.7$ is the mass fraction of hydrogen for the solar abundance. Substitution of above expressions for Eq. (31) yields the radius where hydrogen begins to recombine as

$$r \simeq 8.3 \times 10^3 \left(7.4 + \ln \left[\alpha^{2/5} \dot{m}^{2/5} \dot{m}^{-1/10} r^{3/4} \right] \right)^{4/3} \alpha^{-4/15} \dot{m}^{-4/15} \dot{m}^{2/5} \quad (34)$$

$$\simeq 1.3 \times 10^4 \left(\frac{\alpha}{0.1} \right)^{-4/15} \left(\frac{m}{15} \right)^{-4/15} \left(\frac{\dot{m}}{10^{-3}} \right)^{2/5}. \quad (35)$$

From the first to the second line, we substitute the arguments in the natural logarithm for the typical parameter values $\alpha = 0.1$,⁵ $m = 15$, $\dot{m} = 10^{-3}$, and $r = 10^4$ suggested by Eq. (29). The necessary accretion rate for hydrogen recombination is also obtained by solving Eq. (35) for the mass accretion rate as⁶

$$\dot{m} \simeq 8.0 \times 10^{-15} \left(\frac{\alpha}{0.1} \right)^{2/3} r^{5/2} m^{2/3}. \quad (36)$$

By substituting the above radius into the temperature (32), we obtain

$$T \simeq 1.3 \times 10^4 \text{ K}. \quad (37)$$

This disk temperature corresponds to the effective temperature of

$$T_{\text{eff}} = \left[\frac{3GM\dot{M}}{8\pi\sigma_{\text{SB}}R^3} \right]^{1/4} \simeq 4.5 \times 10^3 \left(\frac{\alpha}{0.1} \right)^{1/5} \left(\frac{m}{15} \right)^{-1/20} \left(\frac{\dot{m}}{10^{-3}} \right)^{-1/20} \text{ K}, \quad (38)$$

where σ_{SB} is the Stefan-Boltzmann constant. The hydrogen recombination temperature (37) should be compared with the temperature of the disks which we consider.

We roughly estimate the temperature of the thin disk part and show that the disk has a low temperature region

⁵ In the hydrogen-ionization instability, the viscous parameter α is assumed to change between the hot and cold branches of the S-curve, in order to explain the outburst amplitude (Mineshige & Osaki 1983; Meyer & Meyer-Hofmeister 1984; Smak 1984). The change of the viscosity parameter is also supported by the detailed analysis of the dwarf-nova observations (Kotko & Lasota 2012), and magnetohydrodynamic simulations of accretion disks (Coleman et al. 2016). In our estimate, we use the viscous parameter $\alpha = 0.1$ in the hot branch.

⁶ When hydrogen recombines and makes the opacity large, convection develops in accretion disks, which decreases the vertical temperature gradient (Meyer & Meyer-Hofmeister 1982; Cannizzo & Wheeler 1984). Therefore, if the convective motion reaches the midplane of the disk, the standard disk formula (32) overestimates the disk temperature. However, Cannizzo & Wheeler (1984) shows that the convection does not reach the midplane at the maximum accretion rate of the S-curve middle branch.

where hydrogen can recombine. We use the standard disk formulae in eq. (32), and evaluate the disk temperature as

$$T \simeq 2.8 \times 10^3 \left(\frac{m}{15} \right)^{-1/5} \left(\frac{\dot{m}}{10^{-3}} \right)^{10/3} \left(\frac{r_{\text{d}}}{10^5} \right)^{-3/4} \left(\frac{\alpha}{0.1} \right)^{-1/5} \text{ K}, \quad (39)$$

where we use the accretion rate and the disk radius of $\dot{m} = 10^{-3}$ and $r_{\text{d}} = 10^5$ which corresponds to BHs with $m = 15$ and $V = 10 \text{ km s}^{-1}$. This value is lower than the hydrogen recombination temperature in Eq. (37). Therefore, the thin disk part of isolated BHs with accretion rate $\dot{m} \gtrsim 10^{-3}$ has the region where hydrogen begins to recombine and makes the disk unstable.

We study the condition of hydrogen recombination more precisely than the above discussion, in particular, on the basis of the disk instability theory (van Paradijs 1996). For an instability to occur, the mass accretion rate should be in the middle branch of the S-curve at some radius. The maximum and minimum accretion rates of the branch are calculated numerically, and fitting formulae are given by Lasota et al. (2008) as⁷

$$\dot{m}_{\text{crit}}^+ = 6.36 \times 10^{-15} \left(\frac{\alpha}{0.1} \right)^{-0.01} r^{2.64} m^{0.75}, \quad (40)$$

$$\dot{m}_{\text{crit}}^- = 3.91 \times 10^{-15} \left(\frac{\alpha}{0.1} \right)^{0.01} r^{2.58} m^{0.73}, \quad (41)$$

where we rewrite the radius and mass from the original notations in Lasota et al. (2008) to the normalized ones, and keep the viscosity parameter α explicitly. It should be noted the numerically obtained maximum accretion rate (40) is roughly reproduced by our analytical formula (36) except for the dependence on the viscosity parameter α . Since the critical rates are increasing functions of radius, for an unstable annulus to exist, the mass accretion rate should be smaller than the maximum rate (40) at the disk radius, $\dot{m} < \dot{m}_{\text{crit}}^+(r = r_{\text{d}})$, and should also be larger than the minimum rate (41) at the transition radius, $\dot{m} > \dot{m}_{\text{crit}}^-(r = r_{\text{tr}})$. For the first condition, the maximum rate at the disk radius is given by

$$\dot{m}_{\text{crit}}^+(r = r_{\text{d}}) = 5.7 \left(\frac{\alpha}{0.1} \right)^{-0.01} \left(\frac{m}{15} \right)^{2.51} \left(\frac{V}{10 \text{ km s}^{-1}} \right)^{-8.8} \quad (42)$$

where we use Eq. (8) for the disk radius. We see that the first condition is easily satisfied. For the second condition, we substitute Eq. (27) to the minimum rate and obtain

$$\dot{m}_{\text{crit}}^-(r = r_{\text{tr}}) = 7.3 \times 10^{-1} \left(\frac{\alpha}{0.1} \right)^{0.01} \left(\frac{m}{15} \right)^{-4.43} \left(\frac{V}{10 \text{ km s}^{-1}} \right)^{15.48} \left(\frac{n}{10^2 \text{ cm}^{-3}} \right)^{-5.16}. \quad (43)$$

At first glance, this condition does not seem to be satisfied. However, for BHs with $\dot{m} \gtrsim 10^{-3}$, the density is larger than $n = 10^2 \text{ cm}^{-3}$, which decrease the minimum rate from the above value. More precisely, to satisfy the second condition, an inequality $(m/15)^{0.88} (n/10^2 \text{ cm}^{-3}) (V/10 \text{ km s}^{-1})^{-3} > 2.9$ should hold. Then, by noting that $\dot{m} \propto m V^{-3} n$, we obtain

⁷ It should be noted that Lasota et al. (2008) mainly studies the stability of helium accretion disks. However, in the Appendix of their paper, they show the fitting formulae for the solar abundance disk, which we use in this work.

the condition for isolated BHs to satisfy the second condition

$$\dot{m} \gtrsim \dot{m}_{\text{XRN}} \approx 3.2 \times 10^{-3} \left(\frac{m}{15}\right)^{0.12} \left(\frac{\epsilon'}{0.63}\right)^{0.84} \left(\frac{1-f}{0.5}\right)^{0.84} \left(\frac{c_1}{0.48}\right)^{1.68} \left(\frac{c_3}{0.32}\right)^{0.84} \left(\frac{\alpha}{0.1}\right)^{1.68} \left(\frac{\beta_{\text{ADAF}}}{0.5}\right)^{-0.42} \quad (44)$$

where we restore the ADAF parameter dependences. In Fig. 2, we also show the required accretion rate for $m = 15$ with a red dashed line.

We conclude that isolated BHs with a mass accretion rate larger than the critical rates (29) and (44) suffer from the hydrogen-ionization instability and cause transient events such as X-ray novae. In Fig. 2, we show the population which causes transients with a red shaded region. We see that the number of the isolated BHs which can produce X-ray novae-like transients by the ionization instability is about $N_{\text{BH}} \sim 20$. BHs in a blue shaded region have mass accretion rates of $\dot{m}_{\text{disk}} < \dot{m} < \dot{m}_{\text{crit}}^-(r = r_{\text{tr}})$. In this case, the whole region of the thin disk parts is always in the cold branch and stable (Menou et al. 1999).

The X-ray novae powered by isolated BHs show similar timescale and luminosity to the observed ones. We briefly estimate the rise and decay timescales and the luminosity of the X-ray novae. Before the detailed estimation, we remark that the accretion rate ($\dot{m} \gtrsim 3 \times 10^{-3}$, see also Fig. 2) and the disk radius ($R_{\text{d}} \sim 10^{11}$ cm for $V \sim 10 \text{ km s}^{-1}$) of the isolated BHs are comparable to those of the X-ray binary system (van Paradijs 1996; Coriat et al. 2012; Remillard & McClintock 2006), which means that the accretion disks in both systems have common properties and show the common outburst signatures. The rise-time is evaluated by the timescale for which a heating-front with velocity $\sim \alpha c_{\text{s,disk}}$ propagates the disk radius (Lasota 2001), as $t_{\text{rise}} \sim R_{\text{d}}/\alpha c_{\text{s,disk}} \sim 10 \text{ days} (R_{\text{d}}/10^{11} \text{ cm})(\alpha/0.1)^{-1} (c_{\text{s,disk}}/10 \text{ km s}^{-1})^{-1}$, where $c_{\text{s,disk}}$ is the sound velocity of the disk. The decay-time is estimated by the viscous timescale as $t_{\text{decay}} \sim t_{\text{vis}} \sim R_{\text{d}}^2/3\nu_{\text{vis}}$, where $\nu_{\text{vis}} \approx \alpha c_{\text{s,disk}} H_{\text{disk}}$ is the kinetic viscosity, and H_{disk} is the disk scale height at the disk radius (King & Ritter 1998). Then, the decay timescale is given by $t_{\text{decay}} \sim 40 \text{ days} (R_{\text{d}}/10^{11} \text{ cm})^2 (\alpha/0.1)^{-1} (c_{\text{s,disk}}/10 \text{ km s}^{-1})^{-1} (H_{\text{disk}}/0.1 R_{\text{d}})^{-1}$. Finally, since the outburst luminosity is evaluated by $L_{\text{burst}} \sim \eta \dot{M}_{\text{burst}} c^2$. The accretion rate is given by $\dot{M}_{\text{burst}} \sim \dot{M}_{\text{d}}/t_{\text{vis}}$, where $\dot{M}_{\text{d}} \sim \pi \Sigma R_{\text{d}}^2$ is the disk mass at the beginning of the outburst and Σ is the surface density at the cold branch of the S-curve. The surface density is obtained by solving the disk structure, but we evaluate it by using the fitting formula developed by Lasota et al. (2008) (their Eq. A.1) as $\Sigma \sim 6 \times 10^2 \text{ g cm}^{-2} (\alpha/0.1)^{-0.83} (R_{\text{d}}/10^{11} \text{ cm})^{1.18} (M_{\text{BH}}/10 M_{\odot})^{-0.40}$. Then, the accretion rate and the luminosity are estimated as $\dot{M}_{\text{burst}} \sim 6 \times 10^{18} \text{ g s}^{-1} (\Sigma/6 \times 10^2 \text{ g cm}^{-2}) (R_{\text{d}}/10^{11} \text{ cm})^2 (t_{\text{vis}}/3 \times 10^6 \text{ s})^{-1}$ and $L_{\text{burst}} \sim 5 \times 10^{38} \text{ erg s}^{-1} (\dot{M}_{\text{burst}}/6 \times 10^{18} \text{ g s}^{-1}) \sim 0.4 L_{\text{Edd}}$ for $M_{\text{BH}} = 10 M_{\odot}$, where $L_{\text{Edd}} = \eta \dot{M}_{\text{Edd}} c^2$ is the Eddington luminosity. The above estimated values of the rise and decay timescales and luminosity agree with the observed values of $t_{\text{rise}} \sim 10 \text{ days}$, $t_{\text{decay}} \sim 30 \text{ days}$, and $L_{\text{burst}} \sim 0.1 L_{\text{Edd}}$ (Chen et al. 1997; Yan & Yu 2015).

Finally, we estimate the event rate and show that the rate is consistent with the observations. We assume that,

in an outburst phase, the BHs have the same luminosity and duration as the observed X-ray novae of $L_{\text{burst}} \approx 0.1 L_{\text{Edd}}$ ($\dot{M}_{\text{burst}} \sim 0.1 \dot{M}_{\text{Edd}}$) and $t_{\text{burst}} \sim t_{\text{rise}} + t_{\text{decay}} \sim 40 \text{ days}$ (Chen et al. 1997; Yan & Yu 2015). To power the outbursts, BHs with $\dot{M} \approx 3 \times 10^{-3} \dot{M}_{\text{Edd}}$ should continue to accrete mass with a duration of

$$t_{\text{quiet}} \sim \frac{t_{\text{burst}} \dot{M}_{\text{burst}}}{\dot{M}}, \quad (45)$$

$$\approx 1300 \left(\frac{t_{\text{burst}}}{40 \text{ d}}\right) \left(\frac{\dot{M}_{\text{burst}}}{0.1 \dot{M}_{\text{Edd}}}\right) \left(\frac{\dot{M}}{3 \times 10^{-3} \dot{M}_{\text{Edd}}}\right)^{-1} \text{ da} \quad (46)$$

It should be noted that the derived duration is less than the dynamical timescale of a BH to cross the Bondi radius t_{dyn} for $V = 10 \text{ km s}^{-1}$, which corresponds to the angular momentum flip timescale of the disk. Then, the event rate is estimated as

$$\frac{N_{\text{BH}}}{t_{\text{quiet}}} \approx 5.5 \left(\frac{N_{\text{BH}}}{20}\right) \left(\frac{t_{\text{burst}}}{40 \text{ d}}\right)^{-1} \left(\frac{\dot{M}_{\text{burst}}}{0.1 \dot{M}_{\text{Edd}}}\right)^{-1} \left(\frac{\dot{M}}{3 \times 10^{-3} \dot{M}_{\text{Edd}}}\right)^{-1} \text{ yr}^{-1}. \quad (47)$$

Interestingly, this value is comparable to the rate of the observed X-ray novae (\sim a few yr^{-1} , Chen et al. 1997; Corral-Santana et al. 2016). Therefore, a part of X-ray novae may be produced by isolated BHs. In order to study this possibility, we need deep and multi-wavelength follow-up observations to confirm whether X-ray novae occur in molecular clouds, and whether there are companion stars or not.

4 DISCUSSION

We discuss the observational strategy to confirm whether an X-ray nova is produced by an isolated BH or not. The simplest way is to exclude companion (or secondary) stars by follow-up observation. Typically, secondary stars of low mass BH X-ray binaries are K- or M-type dwarfs (Remillard & McClintock 2006). Their effective temperature and radius are about $T_{\text{eff}} \sim 4000 \text{ K}$ and $R_* \sim 0.5 R_{\odot}$ (Torres et al. 2010).

Then, we estimate the apparent magnitudes for optical V - ($\lambda_V = 0.545 \mu\text{m}$) and near infrared J - ($\lambda_J = 1.215 \mu\text{m}$), H - ($\lambda_H = 1.654 \mu\text{m}$), and K_s -bands ($\lambda_{K_s} = 2.157 \mu\text{m}$) of the companion stars taking the extinction into account. We set the distance to an isolated BH $d \sim 4 \text{ kpc}$, which is a typical distance to dynamically confirmed BHs (Corral-Santana et al. 2016). For this distance, the hydrogen column density contributed from the interstellar space, amounts to $N_{\text{H}} \sim 1.2 \times 10^{22} (n/1 \text{ cm}^{-3})(d/4 \text{ kpc}) \text{ cm}^{-2}$, where n denotes the number density of the interstellar space. On the other hand, the column density of the molecular clouds where the BH resides, is $N_{\text{H}} \sim 0.9 \times 10^{22} (n/10^2 \text{ cm}^{-3})(l/30 \text{ pc}) \text{ cm}^{-2}$, where we use a typical molecular cloud size of $l \sim 30 \text{ pc}$ (Miville-Deschênes et al. 2017). We see that these contributions are comparable, and we set the total column density as $N_{\text{H}} = 2 \times 10^{22} \text{ cm}^{-2}$ to estimate the extinction. For the column density, the extinction of each band results in $A_V \approx 12 \text{ mag}$, $A_J \approx 3.2 \text{ mag}$, $A_H \approx 2.0 \text{ mag}$ and $A_{K_s} \approx 1.4 \text{ mag}$, where we use $A_{\lambda}/N_{\text{H}} \approx 6.0, 1.6, 1.0$, and $0.7 \times 10^{-22} \text{ cm}^2 \text{ mag}$ for V -, J -, H -, and K_s -bands, respectively (Draine 2003). Then, the apparent magnitudes in these bands become $V \approx 33.6 \text{ mag}$, $J \approx 23.4 \text{ mag}$, $H \approx 22.3 \text{ mag}$ and $K_s \approx 21.9 \text{ mag}$. We find that

optical follow-up observations are extremely difficult to detect secondary stars.

We discuss an observational strategy to confirm the absence of companions in near infrared bands. When an X-ray nova is produced by a binary system, we can find the secondary star by deep near infrared follow-ups. In the actual observations, we can use rough estimations of the column density by using the absorption signature of the soft X-ray spectrum (Liu et al. 2007; Corral-Santana et al. 2016, and references therein), in order to evaluate the necessary depths for follow-ups. In Fig. 3, we show the required depth to detect companion stars if they exist. Some observed X-ray novae whose column densities are evaluated by fitting of the absorbed soft X-ray spectrum (Corral-Santana et al. 2016, and references therein) are also shown. The selected X-ray novae are located at the low galactic latitude position $b \lesssim 1.5^\circ$ because their host molecular clouds have small scale heights (see Table 1). Horizontal dotted lines represent the column density of each transient. Red, green, blue, and magenta curves show the estimated apparent AB magnitude, when the companions are located at 4 kpc from Sun, including extinction in V-, J-, H-, and K_s -bands, respectively. For example, *MAXI J1543-564* has a column density of $\approx 1.4 \times 10^{22} \text{ cm}^{-2}$. With this density, we should conduct follow-up observations as deep as ~ 22.5 , 21.6, and 21.4 mag in J-, H-, K_s -bands. If we can not detect any sources, the transient could be launched by an isolated BH.

It should be also noted that a detection of near infrared sources does not necessarily mean the existence of the companion. We also detect the disk as a near infrared source. In this case, we should conduct spectroscopic observations. When the near infrared source is not the companion but the disk emission of an isolated BH, we do not detect any periodic variation of emission or absorption lines (e.g., H β and He II emission lines, or neutral metals and molecular absorption lines, as actually observed in BH binary systems Khargharia et al. 2010). In a catalog of BH X-ray novae (Corral-Santana et al. 2016), such near infrared candidate sources without periodic variabilities have been already reported, e.g. *IGR J17454-2919*, *XTE J1908-094*, and *SAX J1711.6-3808*. Among these X-ray novae, *IGR J17454-2919* (Paizis et al. 2015) and *SAX J1711.6-3808* (Wang & Wang 2014) are located at the same positions where the near infrared sources have already been detected in the past survey observations, although the positions are crowded with stars and the chance of coincidence is high. Further follow-up observations are not conducted. For the other X-ray nova, *XTE J1908-094* (Chaty et al. 2006), only photometric observations were conducted, and any detections of periodic variabilities were not reported. We should conduct deeper and more careful photometric and spectroscopic observations for these objects.

Radio follow-up observations are also important to study whether the transients are accompanied by molecular clouds or not. For example, the X-ray source *1E 1740.7-2942* in the Galactic center was first proposed to be in a giant molecular cloud by radio observations (Bally & Leventhal 1991; Mirabel et al. 1991), but later shown to be located behind the cloud by detailed X-ray spectroscopic observations (Churazov et al. 1996).

We also discuss the feedback effect of isolated BHs on the event rate. Theoretical studies suggests that

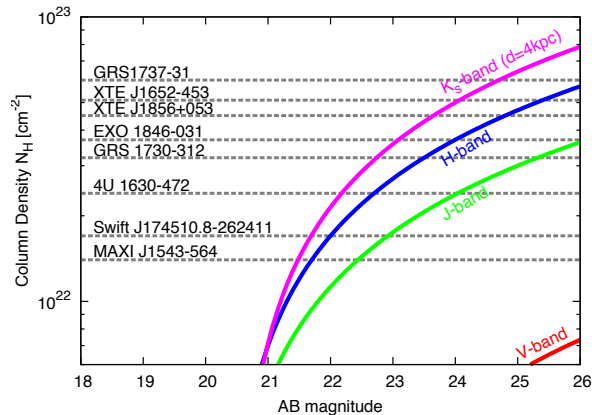


Figure 3. The required depth to detect the companion stars of the observed X-ray novae with the measured column densities. Red, green, blue, and magenta curves show the apparent magnitude of the companion stars, when the companions whose temperature and photospheric radius of $T_{\text{eff}} \sim 4000 \text{ K}$ and $R_* \sim 0.5 R_\odot$, are located at 4 kpc from Sun. The horizontal dotted lines represent the measured column densities for X-ray novae which are not confirmed to have companions.

ADAF solutions allow outflows from the disk systems (Blandford & Begelman 1999, 2004; Yuan et al. 2015). Even a small fraction of accretion mass is blown away, the outflow affects the medium around the Bondi radius (Ioka et al. 2017). When the feedback works, the accretion rate is decreased, which also makes the outflows weak. Ioka et al. (2017) estimated the duty cycle of the self-regulation is about $\sim 1/10$. In this case, the event rate of X-ray novae produced by isolated BHs will be decreased by $\sim 1/10$.

When an X-ray flux from the inner disk part is large, it may affect the disk structure (van Paradijs 1996). The X-rays ionize hydrogen and the Saha equation (30) does not give a correct degree of ionization. Dubus et al. (1999) studied the effect of the X-ray irradiation and concluded that the disk structure nor the S-curve do not change so much in the quiescent state. However, if the accretion disk is warped or there is a X-ray irradiation source above the disk plane, the X-ray ionization may affect the hot branch in the S-curve. This is an interesting future work.

Finally, we remark the difference between our work and Agol & Kamionkowski (2002) who also discussed a probability that isolated BHs launches X-ray novae. They calculated the event rate of X-ray novae produced by isolated BHs by using the mass accretion distribution. Their calculation predicted much more event rate than the observed one, and they concluded that X-ray novae caused by isolated BHs are unlikely. However, they did not consider the disk structure and the instability condition, and extremely underestimate the minimum accretion rate needed to produce X-ray novae. This is why Agol & Kamionkowski (2002) overestimated the event rate of X-ray novae powered by isolated BHs.

ACKNOWLEDGEMENTS

We are thankful Aya Bamba and Shota Kisaka for fruitful discussions and comments. We would like to thank Hi-

toshi Negoro for carefully reading the manuscript and giving us useful comments. We also thank Kengo Tachihara, Rei Enokiya, Shu Masuda and Shogo Kobayashi for kindly helping us to check the CO observation map. TM is especially thankful to Takashi Hosokawa for helpful discussions and daily encouragements. This work is supported by Grant-in-Aid for JSPS Research Fellow 17J09895 (TM), KAKENHI 24000004, 24103006, 26247042, 26287051, 17H01126, 17H06131, 17H06357, and 17H06362 (KI).

REFERENCES

- Abbott, B. P., Abbott, R., Abbott, T. D., et al. 2016, *Physical Review Letters*, 116, 061102
- Abbott, B. P., Abbott, R., Abbott, T. D., et al. 2016, *ApJ*, 818, L22
- Abbott, B. P., Abbott, R., Abbott, T. D., et al. 2016, *Physical Review Letters*, 116, 241103
- Abbott, B. P., Abbott, R., Abbott, T. D., et al. 2016, *Physical Review X*, 6, 041015
- Abramowicz, M. A., Chen, X., Kato, S., Lasota, J.-P., & Regev, O. 1995, *ApJ*, 438, L37
- Agol, E., & Kamionkowski, M. 2002, *MNRAS*, 334, 553
- Armitage, P. J., & Natarajan, P. 1999, *ApJ*, 523, L7
- Armstrong, J. W., Rickett, B. J., & Spangler, S. R. 1995, *ApJ*, 443, 209
- Bally, J., & Leventhal, M. 1991, *Nature*, 353, 234
- Barkov, M. V., Khangulyan, D. V., & Popov, S. B. 2012, *MNRAS*, 427, 589
- Blandford, R. D., & Begelman, M. C. 1999, *MNRAS*, 303, L1
- Blandford, R. D., & Begelman, M. C. 2004, *MNRAS*, 349, 68
- Belczynski, K., Bulik, T., Fryer, C. L., et al. 2010, *ApJ*, 714, 1217
- Berkhuijsen, E. M. 1999, *Plasma Turbulence and Energetic Particles in Astrophysics*, 61
- Bondi, H., & Hoyle, F. 1944, *MNRAS*, 104, 273
- Bondi, H. 1952, *MNRAS*, 112, 195
- Cannizzo, J. K., Wheeler, J. C., & Ghosh, P. 1985, *Cataclysmic Variables and Low-Mass X-ray Binaries*, 113, 307
- Cannizzo, J. K., & Wheeler, J. C. 1984, *ApJS*, 55, 367
- Chaty, S., Mignani, R. P., & Israel, G. L. 2006, *MNRAS*, 365, 1387
- Chen, W., Shrader, C. R., & Livio, M. 1997, *ApJ*, 491, 312
- Chevalier, C., & Ilovaisky, S. A. 1998, *A&A*, 330, 201
- Churazov, E., Gilfanov, M., & Sunyaev, R. 1996, *ApJ*, 464, L71
- Coleman, M. S. B., Kotko, I., Blaes, O., Lasota, J.-P., & Hirose, S. 2016, *MNRAS*, 462, 3710
- Coriat, M., Fender, R. P., & Dubus, G. 2012, *MNRAS*, 424, 1991
- Corral-Santana, J. M., Casares, J., Muñoz-Darias, T., et al. 2016, *A&A*, 587, A61
- Crutcher, R. M., Wandelt, B., Heiles, C., Falgarone, E., & Troland, T. H. 2010, *ApJ*, 725, 466
- Done, C., Gierliński, M., & Kubota, A. 2007, *A&ARv*, 15, 1
- Draine, B. T. 2003, *ARA&A*, 41, 241
- Draine, B. T. 2011, *Physics of the Interstellar and Intergalactic Medium by Bruce T. Draine*. Princeton University Press, 2011. ISBN: 978-0-691-12214-4,
- Dubus, G., Lasota, J.-P., Hameury, J.-M., & Charles, P. 1999, *MNRAS*, 303, 139
- Esin, A. A., McClintock, J. E., & Narayan, R. 1997, *ApJ*, 489, 865
- Fender, R. P., Maccarone, T. J., & Heywood, I. 2013, *MNRAS*, 430, 1538
- Fujita, Y., Inoue, S., Nakamura, T., Manmoto, T., & Nakamura, K. E. 1998, *ApJ*, 495, L85
- Haywood, M., Lehnert, M. D., Di Matteo, P., et al. 2016, *A&A*, 589, A66
- Heyer, M. H., & Brunt, C. M. 2004, *ApJ*, 615, L45
- Heyer, M., Krawczyk, C., Duval, J., & Jackson, J. M. 2009, *ApJ*, 699, 1092
- Hōshi, R. 1979, *Progress of Theoretical Physics*, 61, 1307
- Hoyle, F., & Lyttleton, R. A. 1939, *Proceedings of the Cambridge Philosophical Society*, 35, 405
- Huang, M., & Wheeler, J. C. 1989, *ApJ*, 343, 229
- Ioka, K., Matsumoto, T., Teraki, Y., Kashiya, K., & Murase, K. 2017, *MNRAS*, 470, 3332
- Kato, S., Fukue, J., & Mineshige, S. 2008, *Black-Hole Accretion Disks — Towards a New Paradigm —*, 549 pages, including 12 Chapters, 9 Appendices, ISBN 978-4-87698-740-5, Kyoto University Press (Kyoto, Japan), 2008.,
- Kauffmann, J., Bertoldi, F., Bourke, T. L., Evans, N. J., II, & Lee, C. W. 2008, *A&A*, 487, 993
- Khargharia, J., Froning, C. S., & Robinson, E. L. 2010, *ApJ*, 716, 1105
- King, A. R., & Ritter, H. 1998, *MNRAS*, 293, L42
- Kotko, I., & Lasota, J.-P. 2012, *A&A*, 545, A115
- Kramer, C., Stutzki, J., Rohrig, R., & Corneliussen, U. 1998, *A&A*, 329, 249
- Kuijken, K., & Gilmore, G. 1989, *MNRAS*, 239, 571
- Kuijken, K., & Gilmore, G. 1989, *MNRAS*, 239, 605
- Larson, R. B. 1981, *MNRAS*, 194, 809
- Lasota, J.-P. 2001, *New Astron. Rev.*, 45, 449
- Lasota, J.-P., Dubus, G., & Kruk, K. 2008, *A&A*, 486, 523
- Liu, Q. Z., van Paradijs, J., & van den Heuvel, E. P. J. 2007, *A&A*, 469, 807
- Matsumoto, T., Teraki, Y., & Ioka, K. 2017, in prep
- Menou, K., Narayan, R., & Lasota, J.-P. 1999, *ApJ*, 513, 811
- Meyer, F., & Meyer-Hofmeister, E. 1982, *A&A*, 106, 34
- Meyer, F., & Meyer-Hofmeister, E. 1984, *A&A*, 132, 143
- Miller-Jones, J. C. A. 2014, *Publ. Astron. Soc. Australia*, 31, e016
- Mineshige, S., & Osaki, Y. 1983, *PASJ*, 35, 377
- Mineshige, S., & Wheeler, J. C. 1989, *ApJ*, 343, 241
- Mirabel, I. F., Paul, J., Cordier, B., Morris, M., & Wink, J. 1991, *A&A*, 251, L43
- Mirabel, I. F., & Rodrigues, I. 2003, *Science*, 300, 1119
- Miville-Deschênes, M.-A., Murray, N., & Lee, E. J. 2017, *ApJ*, 834, 57
- Mouschovias, T. C. 1985, *A&A*, 142, 41
- Narayan, R., & Yi, I. 1994, *ApJ*, 428, L13
- Narayan, R., & Yi, I. 1995, *ApJ*, 452, 710
- Osaki, Y. 1974, *PASJ*, 26, 429
- Paizis, A., Nowak, M. A., Rodriguez, J., et al. 2015, *ApJ*, 808, 34
- van Paradijs, J., & Verbunt, F. 1984, *American Institute of Physics Conference Series*, 115, 49
- van Paradijs, J. 1996, *ApJ*, 464, L139
- Remillard, R. A., & McClintock, J. E. 2006, *ARA&A*, 44, 49
- Repetto, S., Davies, M. B., & Sigurdsson, S. 2012, *MNRAS*, 425, 2799
- Reid, M. J., McClintock, J. E., Narayan, R., et al. 2011, *ApJ*, 742, 83
- Rosolowsky, E. 2005, *PASP*, 117, 1403
- Shakura, N. I., & Sunyaev, R. A. 1973, *A&A*, 24, 337
- Shapiro, S. L., & Lightman, A. P. 1976, *ApJ*, 204, 555
- Shapiro, S. L., & Teukolsky, S. A. 1983, *Research supported by the National Science Foundation*. New York, Wiley-Interscience, 1983, 663 p.,
- Smak, J. 1984, *Acta Astron.*, 34, 161
- Snaith, O. N., Haywood, M., Di Matteo, P., et al. 2014, *ApJ*, 781, L31
- Solomon, P. M., Rivolo, A. R., Barrett, J., & Yahil, A. 1987, *ApJ*, 319, 730
- Svensson, R. 1982, *ApJ*, 258, 335
- Tanaka, Y., & Shibazaki, N. 1996, *ARA&A*, 34, 607
- Teraki, Y. et al. 2017, in prep
- Torres, G., Andersen, J., & Giménez, A. 2010, *A&ARv*, 18, 67

- van Paradijs, J. 1996, ApJ, 464, L139
Wang, X., & Wang, Z. 2014, ApJ, 788, 184
White, N. E., & van Paradijs, J. 1996, ApJ, 473, L25
Williams, J. P., & McKee, C. F. 1997, ApJ, 476, 166
Yan, Z., & Yu, W. 2015, ApJ, 805, 87
Yuan, F., Gan, Z., Narayan, R., et al. 2015, ApJ, 804, 101

This paper has been typeset from a \LaTeX file prepared by the author.